Journal of Colloid and Interface Science xxx (xxxx) xxx

Contents lists available at ScienceDirect

Journal of Colloid and Interface Science

journal homepage: www.elsevier.com/locate/jcis

Regular Article

Atomic-level tungsten doping triggered low overpotential for electrocatalytic water splitting

Mengmeng Jin [a], Jiewei Li [a,*], Jingchang Gao [a], Weilan Liu [a], Jing Han [d], Haimin Liu [a], Da Zhan [b,*], Linfei Lai [a,c,*,*]

[a] Key Laboratory of Flexible Electronics & Institute of Advanced Materials (IAM), Jiangsu National Synergistic Innovation Center for Advanced Materials (SICAM), Nanjing Tech University, 5 XinMofan Road, Nanjing 210009, China
[b] State Key Laboratory of Luminescence and Applications, Changchun Institute of Optics, Fine Mechanics and Physics, Chinese Academy of Sciences, Changchun 130033, China
[c] CINTRA CNRS/NTU/Thales, UMI 3288, 50 Nanyang Drive, 637553, Singapore
[d] School of Public Health, Health Science Center, Xi'an Jiaotong University, Xi'an, Shaanxi 710061, China

GRAPHICAL ABSTRACT

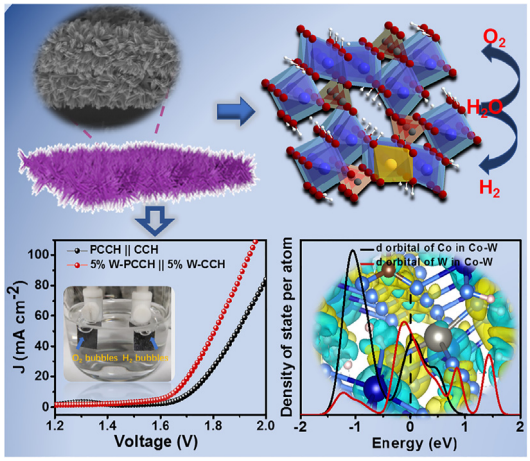

ARTICLE INFO

Article history:
Received 16 September 2020
Revised 3 November 2020
Accepted 4 November 2020
Available online xxxx

Keywords:
Electrochemistry
Heterometal doping
Oxygen evolution reaction
Water splitting

ABSTRACT

The design of electrocatalysts with lower overpotential is of great significance for water splitting. Herein, cobalt hydroxide carbonate (CCH) has been used as a model to demonstrate the boost of its oxygen evolution reaction (OER) activity by atomic doping of W^{6+} (W-CCH). The 5 at % W doping reduced the OER overpotential of CCH by 95.3 mV at 15 mA cm^{-2}, and increased the current density by 2.8 times at 1.65 V. 5%W-PCCH || 5%W-CCH-based electrolyzer only required a potential of 1.65 V to afford 10 mA cm^{-2} for full water splitting. The W^{6+} in CCH are active sites for $O_{\bar{2}}$ adsorption and induced an incesaed electron density near the Fermi level, which facilitates the charge transfer during electrocatalysis. The W^{6+} doping has been validated as an efficient booster for transition-metal carbonate hydroxides-based electrocatalysts, which has half or more than half-filled d-bands.

* Corresponding authors.
E-mail addresses: iamjwli@njtech.edu.cn (J. Li), zhanda@ciomp.ac.cn (D. Zhan), iamlflai@njtech.edu.cn (L. Lai).

https://doi.org/10.1016/j.jcis.2020.11.015
0021-9797/

1. Introduction

Electrocatalytic water splitting for hydrogen and oxygen provides promising energy carrier for clean energy systems, while half-reaction of OER is regarded as the bottleneck [1]. OER involves four successive proton-coupled electron transfer processes in addition to the O—O bond formation and is kinetically sluggish with a high overpotential required [2]. Except for the scarcity and high cost, the unsatisfactory durability of Ir-based electrocatalysts makes the development of new catalysts imperative [3]. The catalytic efficiencies for non-precious metal catalysts are limited by kinetically sluggish surface species adsorption and carrier transfer of the OER [4]. Earth-abundant transition-metal-based electrocatalysts including (Fe, Co, and Ni)-based sulfides [5], oxides [6], hydroxides [7,8], selenides [9], layered double hydroxides (LDHs) [10,11], binary alloy [12,13] and phosphates [14–16] have received considerable research interest in recent years. In particular, the Co and Ni-based hydroxides have been investigated for various electrocatalytic processes, such as OER [17], oxygen reduction [18], hydrogen evolution reaction (HER) [19]. Despite layered structure and redox rich properties, transition metal carbonate hydroxides (MCH), $M_x(OH)_{2(x-1)}CO_3{\cdot}nH_2O$, has been rarely explored as electrocatalyst [20]. Cobalt carbonate hydroxides (CCH) required an overpotential of 0.509 V at a current density of 10 mA cm^{-2} [21], and the construction of a hierarchical structure to increase the catalytic activity by improving the exposure of electroactive sites was unsatisfactory.

To boost the reactivity of active sites and modulate the surface electronic structure toward OER, the combination of Co/Ni-hydroxides with heterometals by doping [22], alloying[23] or constructing heterostructures[24] are required [25]. Fe, Co, Ni-based transition metal can be alloyed with transition metals that have empty or less than half-filled d-bands to achieve a better electrocatalytic activity [26–28]. However, most of these alloys are vulnerable to dissolution or have phase separation concerns during the electrocatalytic process, such as the dissolution of Mo from Co-Mo alloy [29]. Recently, high valence metal species are reported to enable high OER performance due to its low coordination numbers, which facilitate the deprotonation of OOH species to produce O_2 [30]. Zhang et al. reported that the W doping of FeCo hydroxides provides preferable adsorption for OER intermediates [31]. Yan et al. have found the d^0 W^{6+} atoms with a low spin-state has more outermost vacant orbitals to facilitate water and OH^- adsorption on $Ni(OH)_2$ [7]. As a precursor for the synthesis of cobalt oxides, CCH can be easily prepared by a one-step hydrothermal process in high yield in energy-saving conditions such as low temperature, atmospheric pressureand with water as a solvent [32]. It would be a great advance if the intrinsic activity of low-cost CCH can be significantly boosted for wide applications.

Motivated by this, we introduced the atomic level of W^{6+} doping into single crystal orthorhombic CCH *via* a one-step, in-situ hydrothermal method. The 5 at.% of W^{6+} doping can significantly boost the OER performance of CCH, which required an overpotential of 318 mV to reach a current density of 10 mA cm^{-2}. W^{6+} dopant dose has an important effect on the electrocatalytic performance of W-CCH, and catalytic activity enhancement has only been observed at a less than 10 at.% of W doping level. To elucidate the critical role of the tungsten, 5–20 at.% tungsten doped transition metal carbonate hydroxides, such as manganese carbonate hydroxide (W-MnCH), iron carbonate hydroxide (W-FeCH) and nickel carbonate hydroxide (W-NiCH) have been synthesized with their electrocatalytic activity toward OER and HER systematically evaluated. W-CCH has been selected as a demonstrator to show the tunning of electrocatalytic activity by high valence W doping. The substitution of Co in CCH atoms by W is expected to provide more abundant and efficient adsorption sites and accelerate OER kinetics without increasing of the dissociation energy of the products as revealed by DFT calculation. Tungsten doping has been validated as an efficient booster for transition-metal carbonate hydroxides-based electrocatalysts, which have half or more than half-filled d-bands. This concept envisions an efficient strategy for the design of Co, Fe, or Ni-oxides/hydroxide-based catalysts by introducing the atomic percentage of high valence metal doping for challenging multi-electron electrocatalysis.

2. Experimental section

2.1. Materials

All chemicals reagents or materials were used directly without any further purification: cobalt nitrate hexahydrate (99%, Aladdin), ammonium fluoride (98%, Aladdin), urea (>99%, Sinopharm Chemical Reagent Co. Ltd.), ethanol (Wuxi Yasheng Chemical Reagent Co. Ltd.), ammonium metatungstate (>99%, Aladdin).

2.2. The pretreatment of carbon cloth

Commercial carbon cloth was subsequently ultrasonicated in ethanol, acetone, and deionized water for 5 min to remove the impurities. The carbon cloth was further soaked in a 0.5 M nitric acid overnight to improve its hydrophilicity.

2.3. Synthesis of CCH

291 mg of $Co(NO_3)_2$ $6H_2O$, 600 mg of urea, and 371 mg of ammonium fluoride were dissolved in 40 mL of deionized water and stirred for 20 min to form a clear pink solution. The mixture and pretreated carbon cloth (2×3 cm^{-2}) were put into an autoclave for hydrothermal reaction at 120 °C for 6 h. After cooling down to room temperature, the carbon cloth was subsequently rinsed with deionized H_2O and ethanol, and then dried in vacuum at 60 °C to obtain CCH.

2.4. Synthesis of W-CCH

The preparation of W-CCH was similar to that of CCH, except that different amounts of ammonium metatungstate ($H_{28}N_6O_{41}W_{12}$) were added to the precursor solution for hydrothermal reaction. The final samples were denoted as *x*-WCCH, where *x* represented the W to Co molar ratios of the precursors, and *x* corresponded to 2%, 5%, 10%, and 25%.

2.5. Synthesis of W-MCH

The preparation method was similar to CCH. 10 mmol of $MnCO_3$ and 1.15 M urea, 10 mmol $Fe(NO_3)_2$ and 45 mmol urea, 10 mmol $Ni(NO_3)_2$ $6H_2O$ and 480 mg urea and 64 mg of ammonium fluoride were used to synthesis MnCH, FeCH, and NiCH, respectively. Different amount of ammonium metatungstate ($H_{28}N_6O_{41}W_{12}$) to metal ions with molar ratios varied from 1% to 20% were added to the precursor solution to synthesis W-MCH.

2.6. Synthesis of PCCH and 5%W-PCCH

WCCH or CCH was separately placed at one end of a small porcelain boat with 100 mg of NaH_2PO_2 solid at the upstream side of the porcelain boat and annealed at 300 °C for 1 h in Ar, with a temperature ramping rate of 10 °C min^{-1}. 5%W-PCCH and PCCH were washed thoroughly with ethanol and dried in vacuum at 60 °C overnight.

2.7. Material characterization

X-ray diffraction (XRD) patterns of the samples were recorded on Bruker AXS D8 DISCOVER X-ray diffractometer with Cu Kα radiation (=1.5406 Å) at a scanning rate of 1° min^{-1}. Scanning electron microscopy (SEM) images were taken on a JEOL JSM-7800F. Transmission electron microscopy (TEM), selected area electron diffraction (SAED) and high-resolution transmission electron microscopy (HRTEM) were performed on JEM-2010F at an acceleration voltage of 200 kV. X-ray photoelectron spectroscopy (XPS, Esca Lab 250Xi X-ray, Al Kα), inductively coupled plasma optical emission spectrometry (ICP-OES, Optima 8300), and ultraviolet photoelectron spectroscopy (UPS, Thermo Fisher Scientific Esca lab 250xi) were applied to analyze the surface composition and energies in the valence region. The thermogravimetric thermal analysis (TGA) of the samples was performed on Perkin-Elmer, Pyrisl in N_2 atmosphere from 30 °C to 950 °C at a ramping rate of 10 °C min^{-1}.

2.8. Computational details

The first-principles calculations of the density of states and charge density differences were performed in Castep and VASP software, respectively, using a generalized gradient approximation (GGA) method augmented by a Hubbard U term (GGA + U) with PBE functional. The cutoff energy was set at 340 eV, and the atomic positions were relaxed until the energy and force were less than 10^{-5} eV and 3×10^{-3} eV $Å^{-1}$, respectively. The model of W-doped (5%–CCH) was constructed according to the experimental data with one W atom substitute one Co atom in a supercell that has 20 Co atoms.

2.9. Electrochemical measurements

All electrochemical tests were carried out on a CHI760E workstation at room temperature in 1 M KOH. The OER and HER activity of electrodes were evaluated with an as-prepared electrode as a working electrode, graphite rod and Ag/AgCl electrode were applied as counter and the reference electrode, respectively. Electrochemical impedance spectroscopy (EIS) measurements were performed at a frequency from 100 kHz to 0.01 Hz with AC amplitude of 10 mV. The linear voltammetry curves were measured at −0.9 ~ 1.6 V and 0.2 ~ 1.0 V vs. Ag/AgCl for HER and OER reactions at a scan rate of 10 mV s^{-1}, respectively. Chronopotentiometry measurement at the current density 20 mA cm^{-2} was applied to evaluate the stability of the catalysts for HER and OER. All polarization curves were iR corrected, and all potentials were converted into reversible hydrogen electrode (RHE) according to: $E_{RHE} = E_{Ag/AgCl} + 0.059 \times pH + 0.205$.

Water-splitting devices were assembled with 5%W-CCH and 5% W-PCCH as positive and negative electrodes, respectively. The stability of the electrolyzer for overall water splitting was measured by chronopotentiometry at a current density of 10 mA cm^{-2} about 40 h. The electrochemical active surface areas (ESCA) of the CCH and W-CCH electrodes were estimated from the double-layer capacitance (C_{dl}) charging curves *via* cyclic voltammetry [33]. Cyclic voltammograms (CVs) at various scan rates were applied to calculate the C_{dl} within the selected non-Faradaic region (0.48 ~ 0.58 V vs. RHE).

3. Results and discussion

W-doped CCH nanorods have been prepared by the one-step in-situ hydrothermal method with a schematic illustration shown in Fig. 1a. The hydrolysis of urea provided both carbonate and hydroxyl anions to form cobalt hydroxide carbonate [34]. Fluoride anions as effective functional templating agents help the assembly of nanocrystals to form nanoarrays [35]. The reactions to produce hydroxide carbonate can be expressed as follows:

$$H_2NCONH_2 + H_2O \rightarrow 2NH_3 + CO_2 \quad (1)$$

$$CO_2 + H_2O \rightarrow CO_3^{2-} + 2H^+ \quad (2)$$

$$NH_3 + H_2O \rightarrow NH_4^+ + OH^- \quad (3)$$

$$Co^{2+} + OH^- + 0.50CO_3^{2-} + 0..11H_2O \leftrightarrow Co(CO_3)_{0.50}(OH)\cdot 0.11H_2O \quad (4)$$

Fig. 1b-g have shown the scanning electron microscopy (SEM) images of the as-synthesized samples. The surface of CCH is fully covered with W-CCH nanorods with a uniform length of 5 μm. The doping of W barely changes the morphology of CCH, while the density of W-CCH nanoarrays decreases with the increase of W concentration from 10% to 25% (Fig. 1f-g). The W-CCH nanoarray has shown brush-like nanoarrays form bundle-like clusters, while the CCH has an typical needle-like nanoarrayed structure. Transmission electron microscopy (TEM) images (Fig. 1h) have shown that the rod-like 5%W-CCH has an average length of 1–2 μm and a width of 50 to 300 nm. TEM image has demonstrated a rugged surface feature for 5%W-CCH nanorods with the lattice fringes that can be ascribed of the (220) plane of CCH. The doping of W into CCH crystals induced a contraction of (020) plane and expansion of (221) plane (Fig. S1). The corresponding SAED pattern (Fig. 1i) indicated the single crystallinity of CCH nanorod. Darkfield high-resolution TEM and the corresponding elemental mapping have shown the homogeneous distribution of both Co and W in the W-CCH nanorods (Fig. 1j). Inductively coupled plasma mass spectrometry (ICP-MS) analysis of 5%W-CCH revealed the atomic ratio of W was 4.3% for 5% W-CCH, indicating the majority of W precursor was adopted as a doping element for CCH.

XRD patterns (Fig. 2a and S2) indicated both CCH and W-CCH are orthorhombic $Co(CO_3)_{0.50}(OH)\cdot 0.11H_2O$ (JCPDS no. 48–0083). The diffraction patterns of W-CCH have not shown significant deviation from that of CCH; however, the doping of W leads to a red-shifted of (001) plane at ~ 19.9° and a blue-shifted of (221) plane at ~ 33.8°. Therefore, 2–10 at.% of W^{6+} doping did not lead to significant structural deformation or forming side phases due to the lower ionic radii of W^{6+} (0.6 Å) compared with Co^{2+} (0.74 Å), and the low dopant concentration in atomic percentage level. The diffraction peak at ~ 53°, which can be ascribed to the dehydrated cobalt carbonate hydroxides. (JCPDS card, no. 29–1416, $Co_2(OH)_2CO_3$). TGA of CCH and 5% W-CCH are displayed in Fig. S3. The weight loss of CCH and W-CCH from 30 °C to 350 °C is associated with the loss of internal water molecules and hydroxyl groups, including crystal water and absorbed water. Further increasing the temperature from 350 °C to 800 °C leads to a significant weight loss due to the decomposition of carbonate anions groups of CCH, followed by the carbonization of Co_3O_4 to cobaltous oxide (CoO) [34]. The decomposition of carbonate anions groups of 5% W-CCH requires a 10–20 °C higher temperature than that of CCH. The total weight loss of 5% W-CCH (32.20%) is 7.6% less than that of CCH (39.80%), indicating the improved thermal stability of the former. XRD analysis (Fig. S4 and Table S1) of 5% W-CCH after TGA measurement indicate $CoWO_4$ (JCPDS No. 15–0867) and CoO (JCPDS no. 48–1719) are the major products. TGA analysis has demonstrated high thermal stability for W-doped CCH.

X-ray photoelectron spectroscopy (XPS) has been applied to gain insight into the chemical states of W and Co. XPS survey (Fig. 2b) reveals the presence of C, Co, O for CCH and the incorporation of W for W-CCH with the binding energy of 30–40 eV for W 4f orbitals. The high-resolution narrow scan of Co 2p of 5%W-CCH

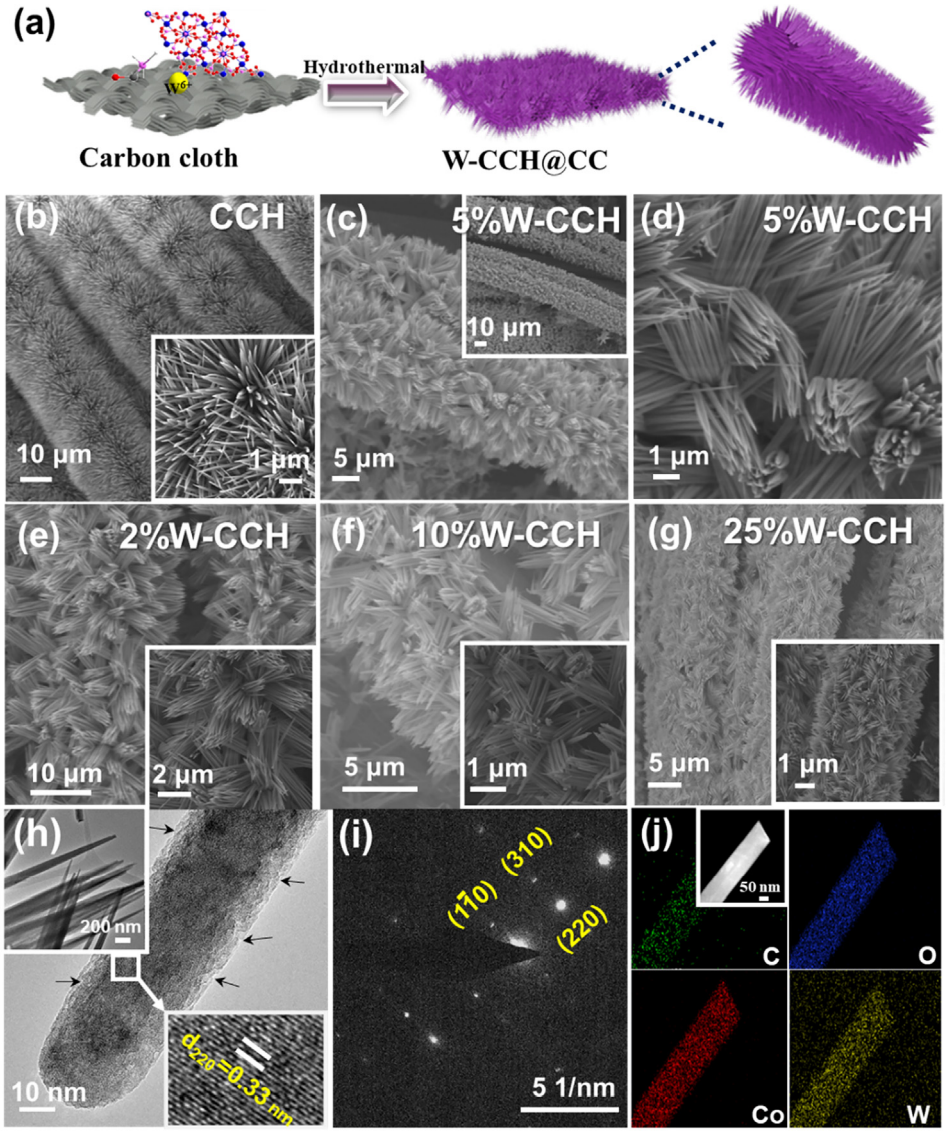

Fig. 1. a) Schematic illustration of the fabrication of CCH and W-CCH. The Co, W, C, O, and H atoms are represented by small blue, yellow, grey, red and white spheres, respectively. b) SEM images of CCH, c-d) 5% W-CCH, e-g) 2–10% W-CCH. h-i) TEM images and SAED pattern of 5%W-CCH, j) EDS mapping of 5%W-CCH and the dark-field HRTEM image (inset). (For interpretation of the references to colour in this figure legend, the reader is referred to the web version of this article.)

(Fig. 2c) has shown four major peaks with two satellites. The peaks at 781.5 and 797.5 eV can be assigned to Co^{2+} [36]. Compared to the CCH, the binding energy of Co $2p_{3/2}$ for Co^{2+} in catalyst has a blue shift by ~ 0.2 eV, indicating W doping does not significantly change the valence of Co but leads to a decreased charge density on Co. The W 4f spectrum (Fig. 2d) with peaks located at 37.5 and 35.6 eV can be ascribed to W^{6+}, and the peaks at 35.3 and 36.6 eV correspond to W^{5+} [37]. W presence as high-valence doping for CCH, and the atomic percentage of W has not changed the crystal structure of CCH.

The electrocatalytic activity of CCH and W-CCH with various molar ratios of W toward OER was evaluated in a typical three-electrode setup. 5%W-CCH has the best catalytic activity among all the samples, delivered a much higher current density than that of the others at the same overpotential (Fig. 3a). 5%W-CCH required overpotentials of 318, 365, and 433 mV to reach current densities of 10, 50, and 200 mA cm^{-2} (Fig. 3b), respectively, while the CCH reference required 332, 391 and 489 mV to reach the same level. The 5%W-CCH has superior catalytic activity than that of W-CCH in 2%, 10%, and 25% of W doping ratios. Moreover, 2%W-CCH, 5%W-CCH, 10%W-CCH and 25%W-CCH have Tafel slopes (Fig. 3c) of 65.67, 65.45, 66.6 and 78.82 mV dec^{-1}, respectively, smaller than that of bare CCH (80.8 mV dec^{-1}). To evaluate the contribution of intrinsic catalytic activity, electrochemically active surface area (ECSA) of the samples estimated from the electrochemical double-layer capacitance (C_{dl}) has been applied to normalize the LSV curves [38]. The characteristic CV cures of W-CCH and CCH at different scan rates are shown in Fig. S5. As shown in Fig. 3d, the increase of W doping from 2% to 10% lead to a gradual decrease of ESCA from 0.5 to 0.35 mF cm^{-2}, all lower than that of bare CCH (0.65 mF cm^{-2}). This suggests the enhanced activity of W-CCH is dominantly caused by the improvement of its intrinsic catalytic activity rather than simply increase its surface area, which facilitating electroactive species adsorption. LSV curves plotted (Fig. 3e) according to the ESCA of each catalyst have clearly shown the excellent catalytic performance of 5%W-CCH. The overpotentials of CCH, 2%W-CCH, 5%W-CCH and 10%W-CCH are 468.4, 426.6, 396.2, and 407.9 mV at 10 mA cm^{-2}, which increased to 513.8, 453.5, 418.6, 430.6 mV at 15 mA cm^{-2}. The 5% doping of W for CCH reduced the overpotential for OER by 72.2 and

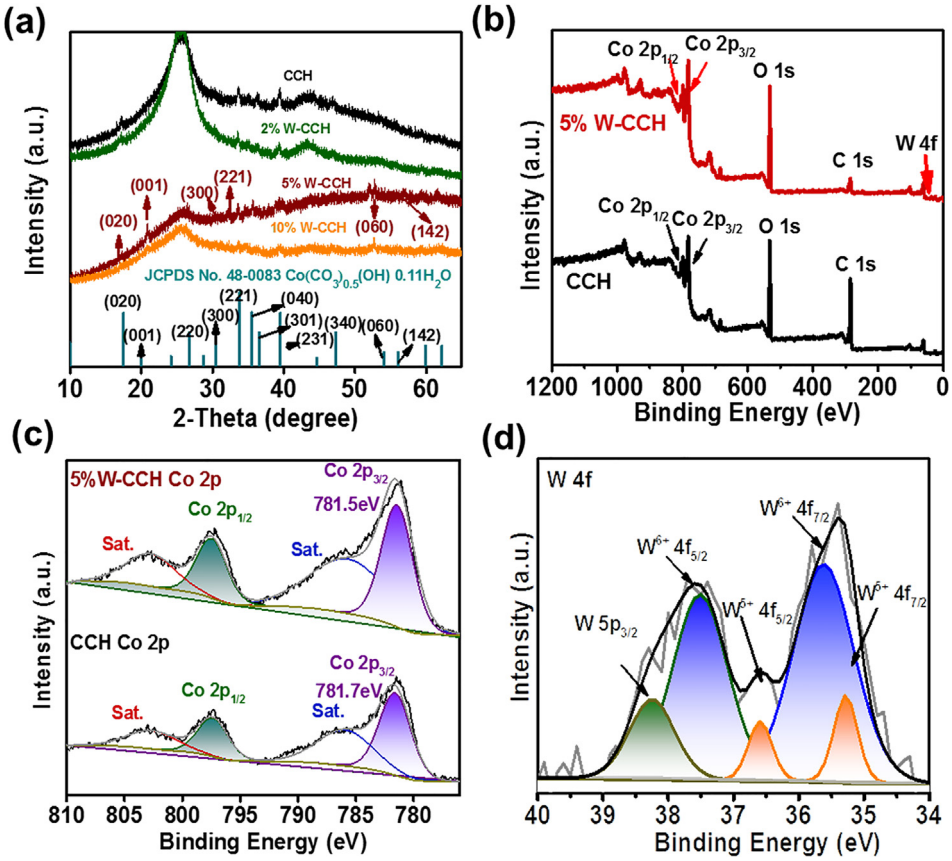

Fig. 2. a) XRD patterns of the CCH and W-CCH with the different molar ratios of W/Co. b) XPS spectra of CCH and 5%W-CCH. d-e) high-resolution XPS Co 2p and W 4f spectra of 5%W-CCH.

95.3 mV to achieve a current of 10 and 15 mA cm^{-2}, respectively. The 5%W-CCH has shown the best catalytic activity among all the samples, delivered a 2.8 times higher specific current density than that of CCH at a 1.65 V vs. RHE (Fig. S6). Nyquist plots normalized to the geometric area of the electrode (Fig. S8) have shown a lower charge-transfer resistance and ion diffusion resistance for 5%W-CCH, indicating a faster OER kinetics. Chronopotentiometric measurement of 5%W-CCH at a constant current of 20 mA cm^{-2} has been applied to evaluate its stability toward water oxidation. The potential of 5%W-CCH maintained at ~ 1.6 V for ~ 40 h without appreciable deactivation, indicating the high electrocatalytic stability of W-CCH (Fig. 3f).

In order to pair with 5% W-CCH for water electrolysis, 5%W-CCH and CCH have been phosphatized with NaH_2PO_2 as the phosphorus source and the as-obtained products were denoted as PCCH and 5% W-PCCH, respectively. Both PCCH and 5%W-PCCH have a nanoarray structure without obvious morphology change compared with those before phosphatization (Fig. S9). XRD patterns (Fig. S10b) of PCCH and 5%W-PCCH display the representative peaks of CoP (JCPDS no. 29–0497). HER activities of as-synthesized samples were measured in 1 M KOH with a graphite rod as the counter electrode. Both PCCH 5%W-PCCH have superior performance than those of CCH and 5%W-CCH, and 5%W-PCCH has shown the highest HER activity (Fig. 4a). The overpotentials required to reach a current density of 10 mA cm^{-2} are 381, 132, 368, and 106 mV for CCH, PCCH, 5%W-CCH, and 5%W-PCCH respectively. Tafel slope (Fig. 4b) of 5%W-PCCH was measured to be 59.0 mV dec^{-1}, lower than of PCCH (62.3 mV dec^{-1}), implying a faster HER kinetics for 5%W-PCCH. Nyquist plots of PCCH and 5%W-PCCH (Fig. S10a) illustrate an improved conductivity after phosphatizing, and 5% W-PCCH has a smaller charge transfer resistance. The long-term stability and durability of 5%W-PCCH were tested by chronopotentiometry method at a current density of 20 mA cm^{-2}. Over 40 h, The current response remains almost unchanged under the continuous operating conditions over 40 h, with an increase of overpotential of 28 mV (Fig. 4c). The polarization curves of PCCH||CCH and 5%W-PCCH||5%W-CCH electrolyzer in 1 M KOH for overall water splitting are shown in Fig. 4c. For 5%W-PCCH||5%W-CCH-based electrolyzer devices, the potential required to catalyze water oxidation at 10 mA cm^{-2} is 1.65 V, outperformed that of PCCH||CCH electrodes (1.72 V). Vigorous oxygen and hydrogen bubbling can also be observed clearly when the two-electrode overall water splitting system was powered (inset Fig. 4d). 5%W-PCCH||5%W-CCH required an overpotential of 318 mV to achieve a current density of 10 mA cm^{-2}, which was among the lowest compared to those recently reported high-performance catalysts based devices [12,39–47] (Fig. 4e), far more exceed that of the industrial standard for water electrolysis voltage (1.8–2.2 V) [48]. The durability of 5% W-PCCH||5%W-CCH-based (Fig. 4f) electrolyzer in 1 M KOH has been investigated, and the decomposition voltage of water only increased by 35 mV after 40 h of continuous electrolysis at a current density 10 mA cm^{-2}. After 40 h of water electrolysis, the voltage of PCCH||CCH-based electrolyzer (Fig. S10d) increased by 200 mV. Based on the above investigations, doping of high-valence W in the atomic percentage level is a facile and effective method to boost the intrinsic catalytic activity of CCH for OER and HER.

Based on the above investigations, doping of high-valence W in the atomic percentage level is effective in boosting the intrinsic catalytic activity of CCH toward OER and HER. To gain in-depth

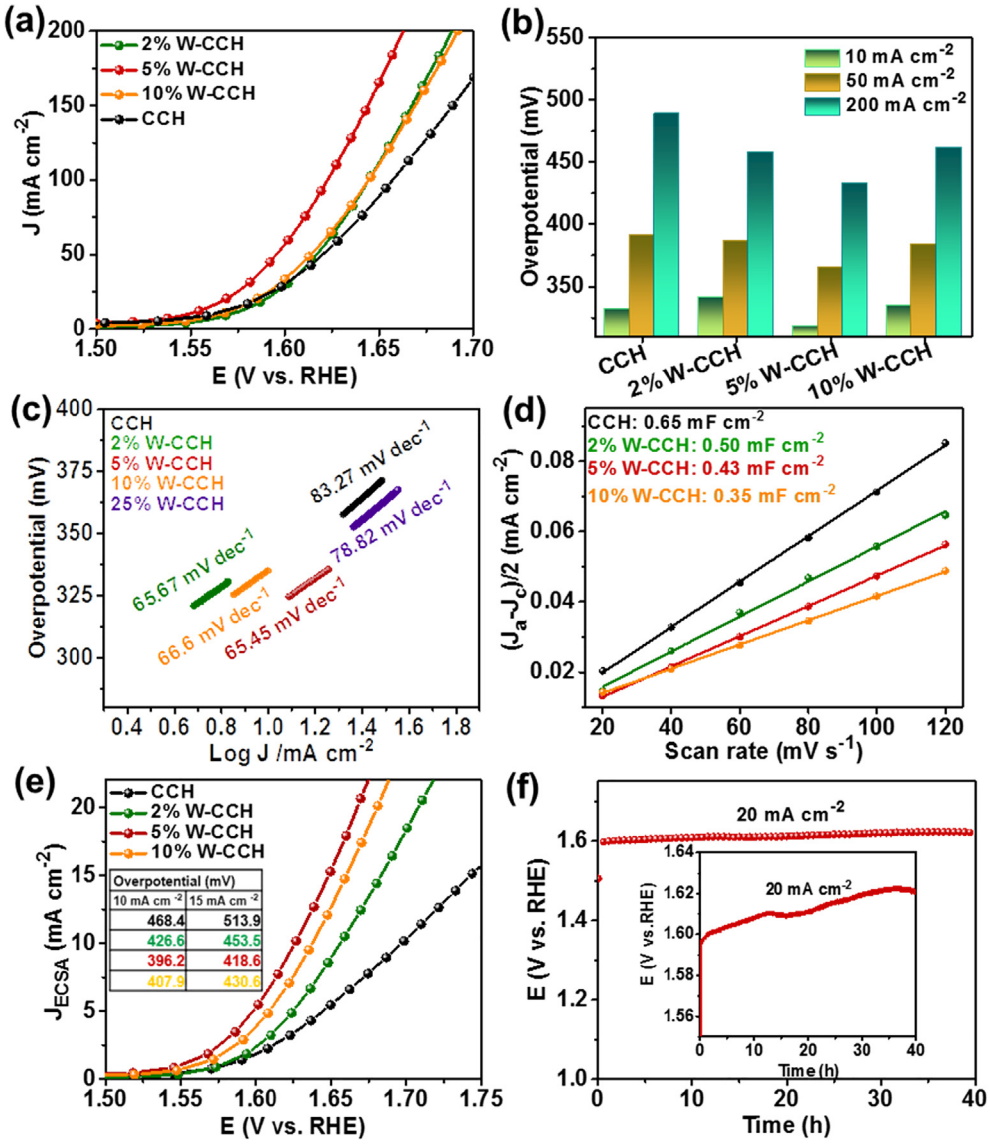

Fig. 3. The OER performance of CCH and W-CCH with different ratios of W to Co. a) The linear polarization curves. b) Overpotentials required for j = 10, 50, and 200 mA cm^{-2}, c) Tafel plots for CCH and W-CCH. d) ESCA calculated by plotting the Δj against the scan rate. e) The LSV curves plotted according to ESCA of each catalyst. f) Chronopotentiometric curve of 5%W-CCH at j = 20 mA cm^{-2} for continuous OER process.

understanding of the underlying mechanism for the enhanced activity of W-doped CCH, valence band structure, and the density functional theory (DFT) calculation have been conducted. Ultraviolet photoelectron spectroscopy (UPS) (Fig. 5a) has shown that the valence band maximum values are ~ 5.22, 5.11, and 5.00 eV for CCH, 5%W-CCH and 10%W-CCH, respectively. Since the valence electrons close to the Fermi level mainly contributes to the d states, the shift of the valence band implied the d-band center of 5%W-CCH also shifts compared to that of CCH [49]. Earlier work has reported the W^{6+} dopant can adjust reactants and intermediates adsorption/desorption, and thereby improve the intrinsic catalytic activity of transition metal compounds [20]. The specific roles of W^{6+} and Co on the catalytic process need to be explored with more experimental and theoretical evidence. DFT was employed to calculate the density of state (DOS) and partial DOS (PDOS) of CCH and W-CCH and further evaluate the overlapping of the d-orbitals of metal atoms after the heterometal doping [50]. The calculations were performed by GGA/PBE method in Castep software with the corresponding models illustrated in Fig. S11a. The d orbital of W positioned near the Fermi level contribute higher state density per atom than that of Co (Fig. 5c), indicating the W dopant facilitates the charge transfer at the catalytic process. In addition, compared with the CCH, the total DOS of W-CCH (Fig. S11b) decrease at around Fermi level, implying the doping of W decreases the energy of Co atoms, thus enabling Co more difficult to lose electron which reduces the energy barrier of O_2-dissociation step. The change of charge density (Fig. 5b) with the cyan and yellow represents depletion and accumulation of electron density, respectively. The W^{6+} dopant barely attracts electron or electron density from Co toward itself. The O atoms adjacent to Co atoms has shown an increase of charge density, indicating the electron donation from Co to π* orbital of O from adsorbed reactants is possible, which can reduce the energy for O_2 dissociation and promote the evolution of O_2. The reduced total density of states for W-CCH also desmontrate the easier desprotion of byproducts from the W-CCH surface. It is noteworthy that the electron density of W^{6+} barely changed after they were adopted as dopants for CCH, indicating the electrophilicity of W has been well maintained, which facilitates surface hydroxyl adsorption and *OOH intermediates formation. The high valence W element

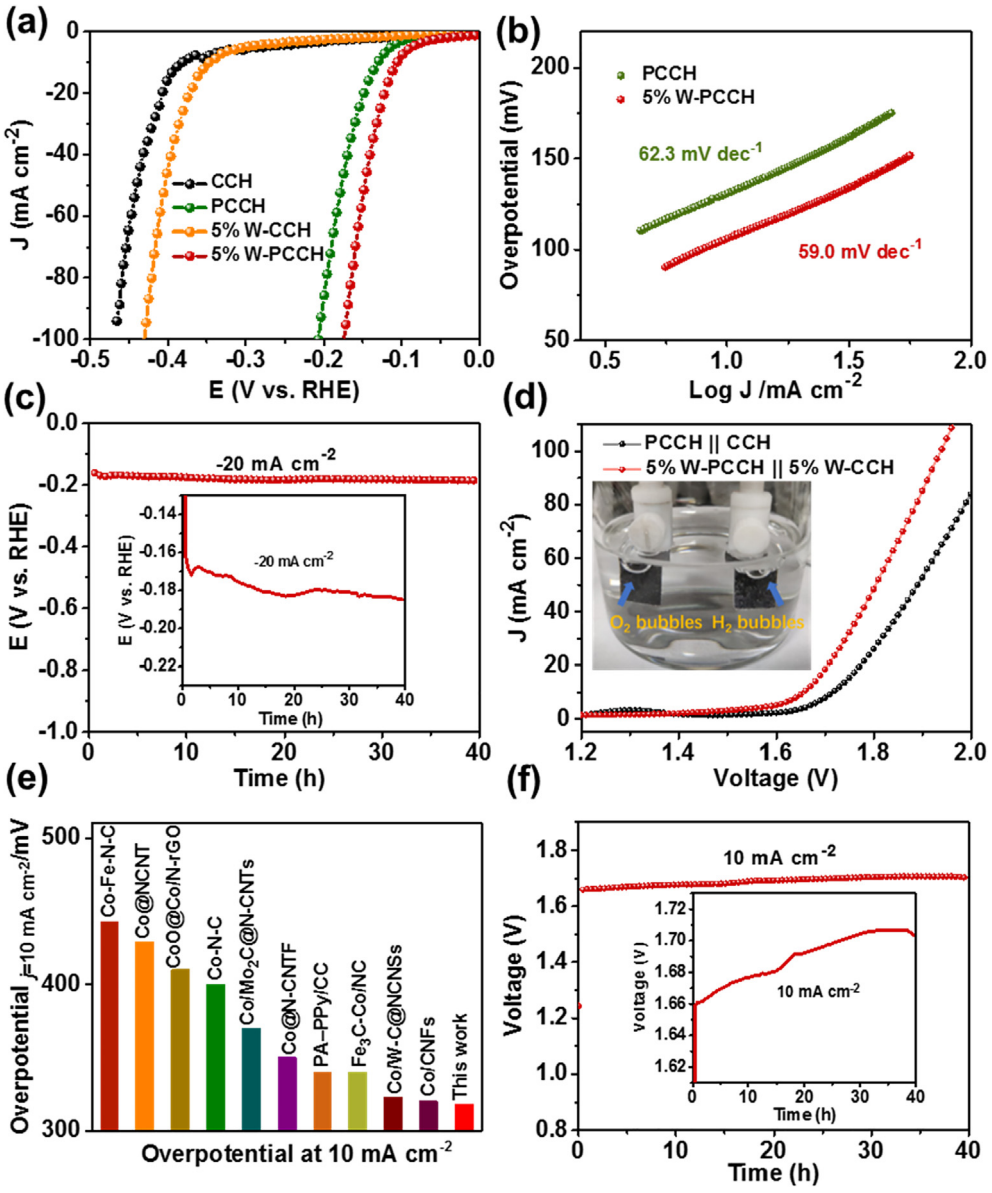

Fig. 4. a) HER polarization curves of CCH, 5%W-CCH, and their corresponding phosphides. b) Tafel plots for PCCH and 5%W-PCCH. c) Chronopotentiometric curve of 5%W-PCCH at j = 20 mA cm^{-2} for continuous HER process. d) The digital photograph and polarization curves of 5%W-PCCH || 5%W-CCH overall water splitting devices. e) Comparison of the overpotential values required for cobalt-based OER catalysts to drive a current density of 10 mA cm^{-2}. f) long-term stability test at 10 mA cm^{-2} over 40 h.

has enough unoccupied outmost electron orbital to bind with water molecules as efficient adsorption sites, while the Co sites reduce the dissociation energy of the products. The W and Co-work synergistically accelerate the OER kinetics and lead to a lower overpotential.

To validate the effect of W^{6+} dopant on the electrocatalytic performance of various types of transition metal carbonate hydroxides, 5–20 at.% of W^{6+} doped MnCH, FeCH, NiCH have been prepared with their OER activity systematically evaluated. Significant improvement can be observed for NiCH, CCH, and FeCH, while the W^{6+} doping is ineffective for MnCH from Fig. S12. The Ni^{2+} and Co^{2+} in NiCH and CCH have a d-electron structure of d8 and d7, respectively. The d5 Fe^{3+} in FeCH has a half-filled d-band, and d4 Mn^{3+} has a less than half-filled d band. The charge transfer process illustrated in Fig. 5d explains how the W^{6+} dopant modifies the charge transfer process of CCH. The e^-- e^- repulsion is the dominant interaction between the bridging O^{2-} and Co^{2+} during the adsorption process of CCH, as the t_{2g} d orbitals of Co^{2+} in the low-spin state are fully occupied [51]. The W^{6+} has empty 5d orbitals, which enable the acceptance of the donation of π electrons from O^{2-} adsorbates. Therefore, the high valence W-dopant is effective adsorption sites for MCH, which has more than half-filled d-bands. However, d4 Mn^{3+} has a less than half-filled d bands, and the W^{6+} doping has shown insignificant improvements for MnCH. The W^{6+} doping is effective in promoting the OER catalysis of MCH, which has half or more than half-filled d-bands, and W^{6+} work as active sites for O_2^- adsorption.

4. Conclusion

Herein, we report the atomic level of W^{6+} doping to boost the intrinsic electrocatalytic performance of CCH. The 5 at.% of W^{6+} doping of CCH boost the specific current density of OER by 2.8 times at a given potential of 1.65 V vs. RHE, and reduce the overpotential for water oxidation by 95.3 mV at a current of 15 mA cm^{-2}. 5%W-PCCH||5%W-CCH-based electrolyzers only required a small potential of 1.65 V to afford a 10 mA cm^{-2} current density for full water splitting. The remarkable performance of W-CCH can be

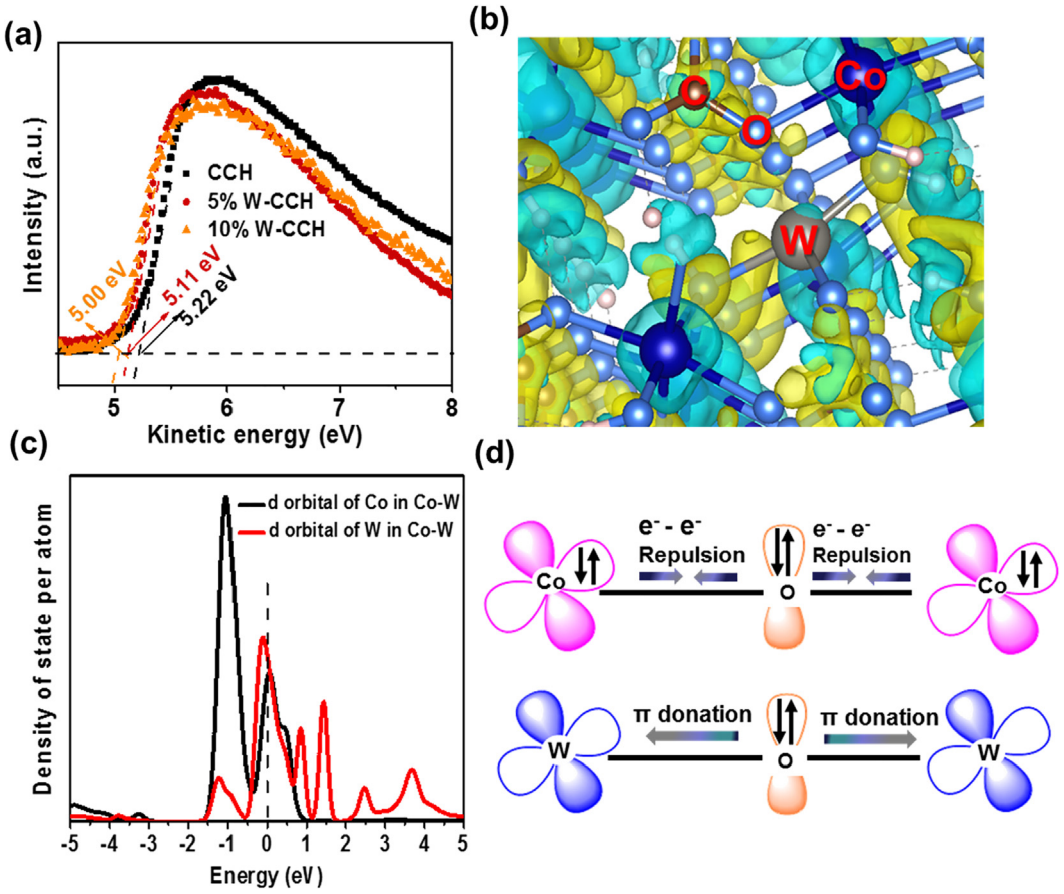

Fig. 5. a) UPS spectra of CCH, 5% W-CCH and 10% W-CCH. b) Charge density differences for Co, W, C, H and O atoms in 5%W-CCH. c) The PDOS of 5%W-CCH. d) Schematic representation of the electronic coupling between Co and W in W-CCH.

ascribed to the atomic percentage of W^{6+} doping into CCH, which promoted the intrinsic catalytic activity of CCH. W^{6+} atoms have abundant vacant orbitals for O_2^- adsorption, while the doping facilitates the desorption of byproducts and reduces the energy barrier for O_2 dissociation. The W^{6+} doping is effective in promoting the OER catalysis of MCH, which has half or more than half-filled d-bands. The remarkable improvement by atomic percentage W^{6+} doping envisions an efficient modulation strategy of electrocatalysts by high valence heterometal doping.

CRediT authorship contribution statement

Mengmeng Jin: Investigation, Data curation, Writing - original draft. **Jiewei Li:** Methodology, Validation. **Jingchang Gao:** Validation. **Weilan Liu:** Formal analysis. **Jing Han:** Writing - review & editing. **Haimin Liu:** Visualization, Methodology. **Da Zhan:** Supervision, Funding acquisition. **Linfei Lai:** Supervision, Writing - review & editing, Methodology, Project administration.

Declaration of Competing Interest

The authors declared that there is no conflict of interest.

Acknowledgments

The work is supported by the CAS Pioneer Hundred Talents Program. We thank Prof. Wei Chen (NUS, Singapore) and Prof. Hongying Mao (HZNU, China) for UPS measurements.

Appendix A. Supplementary data

Supplementary data to this article can be found online at https://doi.org/10.1016/j.jcis.2020.11.015.

References

[1] Z. W. Seh, Jakob Kibsgaard, Colin F. Dickens, Ib Chorkendorff, Jens K. Nørskov, Thomas F. Jaramillo1, Combining theory and experimentin electrocatalysis Insights intomaterials design, Science 355 (2017).
[2] N. Suen, Sung-Fu Hung, Quan Quan, Nan Zhang, Y.-J. Xu*, H.M. Chen, Electrocatalysis for the oxygen evolution reaction recent development and future perspectives, Chem. Soc. Rev. 46 (2017) 337-365.
[3] Q. Shi, C. Zhu, D. Du, Y. Lin, Robust noble metal-based electrocatalysts for oxygen evolution reaction, Chem. Soc. Rev. 48 (12) (2019) 3181–3192.
[4] H. Han, H. Choi, S. Mhin, Y.-R. Hong, K.M. Kim, J. Kwon, G. Ali, K.Y. Chung, M. Je, H.N. Umh, D.-H. Lim, K. Davey, S.-Z. Qiao, U. Paik, T. Song, Advantageous crystalline–amorphous phase boundary for enhanced electrochemical water oxidation, Energy Environ. Sci. 12 (8) (2019) 2443–2454.
[5] H. Li, S. Chen, Y. Zhang, Q. Zhang, X. Jia, Q. Zhang, L. Gu, X. Sun, L. Song, X. Wang, Systematic design of superaerophobic nanotube-array electrode comprised of transition-metal sulfides for overall water splitting, Nat. Commun. 9 (1) (2018) 2452.
[6] A. Bergmann, T.E. Jones, E. Martinez Moreno, D. Teschner, P. Chernev, M. Gliech, T. Reier, H. Dau, P. Strasser, Unified structural motifs of the catalytically active state of Co(oxyhydr)oxides during the electrochemical oxygen evolution reaction, Nat. Catalysis 1 (9) (2018) 711–719.
[7] J. Yan, L. Kong, Y. Ji, J. White, Y. Li, J. Zhang, P. An, S. Liu, S.T. Lee, T. Ma, Single atom tungsten doped ultrathin α-$Ni(OH)_2$ for enhanced electrocatalytic water oxidation, Nat. Commun. 10 (1) (2019) 2149.
[8] Z.W. Gao, J.Y. Liu, X.M. Chen, X.L. Zheng, J. Mao, H. Liu, T. Ma, L. Li, W.C. Wang, X.W. Du, Engineering NiO/NiFe LDH Intersection to Bypass Scaling Relationship for Oxygen Evolution Reaction via Dynamic Tridimensional Adsorption of Intermediates, Adv. Mater. 31 (11) (2019) e1804769.
[9] G. Yilmaz, C.F. Tan, Y.-F. Lim, G.W. Ho, Pseudomorphic Transformation of Interpenetrated Prussian Blue Analogs into Defective Nickel Iron Selenides for

Enhanced Electrochemical and Photo-Electrochemical Water Splitting, Adv. Energy Mater. 9 (1) (2019) 1802983.
[10] L. Zhou, M. Guo, Y. Li, Q. Gu, W. Zhang, C. Li, F. Xie, D. Lin, Q. Zheng, One-step synthesis of wire-in-plate nanostructured materials made of CoFe-LDH nanoplates coupled with $Co(OH)_2$ nanowires grown on a Ni foam for a high-efficiency oxygen evolution reaction, Chem. Commun. (Camb.) 55 (29) (2019) 4218–4221.
[11] K. He, T. Tadesse Tsega, X. Liu, J. Zai, X.H. Li, X. Liu, W. Li, N. Ali, X. Qian, Utilizing the Space-Charge Region of the FeNi-LDH/CoP p-n Junction to Promote Performance in Oxygen Evolution Electrocatalysis, Angew. Chem. Int. Ed. Engl. 58 (34) (2019) 11903–11909.
[12] L. Bai, C.S. Hsu, D.T.L. Alexander, H.M. Chen, X. Hu, A Cobalt-Iron Double-Atom Catalyst for the Oxygen Evolution Reaction, J. Am. Chem, Soc, 2019.
[13] Y. Xiong, Y. Yang, F.J. DiSalvo, H.D. Abruna, Metal-Organic-Framework-Derived Co-Fe Bimetallic Oxygen Reduction Electrocatalysts for Alkaline Fuel Cells, J. Am. Chem. Soc. 141 (27) (2019) 10744–10750.
[14] S.-S. Lu, L.-M. Zhang, Y.-W. Dong, J.-Q. Zhang, X.-T. Yan, D.-F. Sun, X. Shang, J.-Q. Chi, Y.-M. Chai, B. Dong, Tungsten-doped Ni–Co phosphides with multiple catalytic sites as efficient electrocatalysts for overall water splitting, J. Mater. Chem. A 7 (28) (2019) 16859–16866.
[15] P.W. Menezes, C. Panda, C. Walter, M. Schwarze, M. Driess, A Cobalt-Based Amorphous Bifunctional Electrocatalysts for Water-Splitting Evolved from a Single-Source Lazulite Cobalt Phosphate, Adv. Funct. Mater. 29 (32) (2019) 1808632.
[16] H. Liu, M. Jin, D. Zhan, J. Wang, X. Cai, Y. Qiu, L. Lai, Stacking faults triggered strain engineering of ZIF-67 derived Ni-Co bimetal phosphide for enhanced overall water splitting, Appl. Catal. B 272 (2020) 118951.
[17] Z. Xue, X. Zhang, J. Qin, R. Liu, Revealing Ni-based layered double hydroxides as high-efficiency electrocatalysts for the oxygen evolution reaction: a DFT study, J. Mater. Chem. A 7 (40) (2019) 23091–23097.
[18] B. Ni, P. He, W. Liao, S. Chen, L. Gu, Y. Gong, K. Wang, J. Zhuang, L. Song, G. Zhou, X. Wang, Surface Oxidation of AuNi Heterodimers to Achieve High Activities toward Hydrogen/Oxygen Evolution and Oxygen Reduction Reactions, Small 14 (14) (2018) 1703749.
[19] L. Hui, Y. Xue, D. Jia, H. Yu, C. Zhang, Y. Li, Multifunctional Single-Crystallized Carbonate Hydroxides as Highly Efficient Electrocatalyst for Full Water splitting, Adv. Energy Mater. 8 (20) (2018) 1800175.
[20] T. Tang, W.J. Jiang, S. Niu, N. Liu, H. Luo, Y.Y. Chen, S.F. Jin, F. Gao, L.J. Wan, J.S. Hu, Electronic and Morphological Dual Modulation of Cobalt Carbonate Hydroxides by Mn Doping toward Highly Efficient and Stable Bifunctional Electrocatalysts for Overall Water Splitting, J. Am. Chem. Soc. 139 (24) (2017) 8320–8328.
[21] Y. Wang, W. Ding, S. Chen, Y. Nie, K. Xiong, Z. Wei, Cobalt carbonate hydroxide/C: an efficient dual electrocatalyst for oxygen reduction/evolution reactions, Chem Commun (Camb) 50(98) (2014) 15529-32.
[22] U.K. Sultana, J.D. Riches, A.P. O'Mullane, Gold Doping in a Layered Co-Ni Hydroxide System via Galvanic Replacement for Overall Electrochemical Water Splitting, Adv. Funct. Mater. 28 (43) (2018) 1804361.
[23] L.-K. Wu, W.-Y. Wu, J. Xia, H.-Z. Cao, G.-Y. Hou, Y.-P. Tang, G.-Q. Zheng, A nanostructured nickel–cobalt alloy with an oxide layer for an efficient oxygen evolution reaction, J. Mater. Chem. A 5 (21) (2017) 10669–10677.
[24] H. Zhang, X. Li, A. Hähnel, V. Naumann, C. Lin, S. Azimi, S.L. Schweizer, A.W. Maijenburg, R.B. Wehrspohn, Bifunctional Heterostructure Assembly of NiFe LDH Nanosheets on NiCoP Nanowires for Highly Efficient and Stable Overall Water Splitting, Adv. Funct. Mater. 28 (14) (2018) 1706847.
[25] X. Zhang, J. Li, Y. Yang, S. Zhang, H. Zhu, X. Zhu, H. Xing, Y. Zhang, B. Huang, S. Guo, E. Wang, $Co_{3\ O}4$ /$F_{e0.3}3$ $C_{o0.6}6$ P Interface Nanowire for Enhancing Water Oxidation Catalysis at High Current Density, Adv. Mater. 30 (45) (2018) e1803551.
[26] M. Luo, S. Guo, Strain-controlled electrocatalysis on multimetallic nanomaterials, Nat. Rev. Mater. 2 (11) (2017).
[27] S. Schnur, A. Groß, Strain and coordination effects in the adsorption properties of early transition metals: A density-functional theory study, Physical Rev, B 81 (3) (2010).
[28] Q. Xia, H. Liu, M. Jin, L. Lai, Y. Qiu, H. Zhai, H. Li, X. Liu, Catalysts confined inside CNTs derived from 2D metal–organic frameworks for electrolysis, Nanoscale (2020).
[29] C.R. Lee, S.G. Kang, Electrochemical stability of Co-Mo intermetallic compound electrodes for hydrogen oxidation reaction in hot KOH solution, J. Power Sources 87 (1–2) (2000) 64–68.
[30] M. Tahir, L. Pan, R.R. Zhang, Y.C. Wang, G.Q. Shen, I. Aslam, M.A. Qadeer, N. Mahmood, W. Xu, L. Wang, X.W. Zhang, J.J. Zou, High-Valence-State NiO/Co_3O_4 Nanoparticles on Nitrogen-Doped Carbon for Oxygen Evolution at Low Overpotential, ACS Energy Lett. 2 (9) (2017) 2177–2182.
[31] B. Zhang, X.L. Zheng, O. Voznyy, R. Comin, M. Bajdich, M. Garcia-Melchor, L.L. Han, J.X. Xu, M. Liu, L.R. Zheng, F.P.G. de Arquer, C.T. Dinh, F.J. Fan, M.J. Yuan, E. Yassitepe, N. Chen, T. Regier, P.F. Liu, Y.H. Li, P. De Luna, A. Janmohamed, H.L.L. Xin, H.G. Yang, A. Vojvodic, E.H. Sargent, Homogeneously dispersed multimetal oxygen-evolving catalysts, Science 352 (6283) (2016) 333–337.
[32] X. Han, C. Yu, H. Huang, W. Guo, C. Zhao, H. Huang, S. Li, Z. Liu, X. Tan, Z. Gao, J. Yu, J. Qiu, Phase controllable synthesis of Ni^{2+} post-modified CoP nanowire for enhanced oxygen evolution, Nano Energy 62 (2019) 136–143.
[33] E.L. Clark, J. Resasco, A. Landers, J. Lin, L.-T. Chung, A. Walton, C. Hahn, T.F. Jaramillo, A.T. Bell, Standards and Protocols for Data Acquisition and Reporting for Studies of the Electrochemical Reduction of Carbon Dioxide, ACS Catal. 8 (7) (2018) 6560–6570.
[34] S.L. Wang, L.Q. Qian, H. Xu, G.L. Lü, W.J. Dong, W.H. Tang, Synthesis and structural characterization of cobalt hydroxide carbonate nanorods and nanosheets, J. Alloy. Compd. 476 (1–2) (2009) 739–743.
[35] Y. Zhang, B. Ouyang, J. Xu, G. Jia, S. Chen, R.S. Rawat, H.J. Fan, Rapid Synthesis of Cobalt Nitride Nanowires: Highly Efficient and Low-Cost Catalysts for Oxygen Evolution, Angew. Chem. Int. Ed. 55 (30) (2016) 8670–8674.
[36] L. Ma, S. Chen, H. Li, Z. Ruan, Z. Tang, Z. Liu, Z. Wang, Y. Huang, Z. Pei, J.A. Zapien, C. Zhi, Initiating a mild aqueous electrolyte Co_3O_4/Zn battery with 2.2 V-high voltage and 5000-cycle lifespan by a Co(iii) rich-electrode, Energy Environ. Sci. 11 (9) (2018) 2521–2530.
[37] D. Gao, R. Liu, J. Biskupek, U. Kaiser, Y.F. Song, C. Streb, Modular Design of Noble-Metal-Free Mixed Metal Oxide Electrocatalysts for Complete Water Splitting, Angew. Chem. Int. Ed. Engl. 58 (14) (2019) 4644–4648.
[38] D. Voiry, M. Chhowalla, Y. Gogotsi, N.A. Kotov, Y. Li, R.M. Penner, R.E. Schaak, P. S. Weiss, Best Practices for Reporting Electrocatalytic Performance of Nanomaterials, ACS Nano 12 (10) (2018) 9635–9638.
[39] T. Zhao, J. Gao, J. Wu, P. He, Y. Li, J. Yao, Highly Active Cobalt/Tungsten Carbide@N-Doped Porous Carbon Nanomaterials Derived from Metal-Organic Frameworks as Bifunctional Catalysts for Overall Water Splitting, Energy Technology 7 (4) (2019) 1800969.
[40] H. Guo, Q. Feng, J. Zhu, J. Xu, Q. Li, S. Liu, K. Xu, C. Zhang, T. Liu, Cobalt nanoparticle-embedded nitrogen-doped carbon/carbon nanotube frameworks derived from a metal–organic framework for tri-functional ORR, OER and HER electrocatalysis, J. Mater. Chem. A 7 (8) (2019) 3664–3672.
[41] Q. Hu, G. Li, X. Liu, B. Zhu, X. Chai, Q. Zhang, J. Liu, C. He, Superhydrophilic Phytic-Acid-Doped Conductive Hydrogels as Metal-Free and Binder-Free Electrocatalysts for Efficient Water Oxidation, Angew. Chem. Int. Ed. Engl. 58 (13) (2019) 4318–4322.
[42] X.X. Liu, J.B. Zang, L. Chen, L.B. Chen, X. Chen, P. Wu, S.Y. Zhou, Y.H. Wang, A microwave-assisted synthesis of CoO@Co core–shell structures coupled with N-doped reduced graphene oxide used as a superior multi-functional electrocatalyst for hydrogen evolution, oxygen reduction and oxygen evolution reactions, J. Mater. Chem. A 5 (12) (2017) 5865–5872.
[43] T. Ouyang, Y.Q. Ye, C.Y. Wu, K. Xiao, Z.Q. Liu, Heterostructures Composed of N-Doped Carbon Nanotubes Encapsulating Cobalt and β-Mo_2 C Nanoparticles as Bifunctional Electrodes for Water Splitting, Angew. Chem. Int. Ed. Engl. 58 (15) (2019) 4923–4928.
[44] Z. Pei, Z. Tang, Z. Liu, Y. Huang, Y. Wang, H. Li, Q. Xue, M. Zhu, D. Tang, C. Zhi, Construction of a hierarchical 3D Co/N-carbon electrocatalyst for efficient oxygen reduction and overall water splitting, J. Mater. Chem. A 6 (2) (2018) 489–497.
[45] C.C. Yang, S.F. Zai, Y.T. Zhou, L. Du, Q. Jiang, Fe_3C-Co Nanoparticles Encapsulated in a Hierarchical Structure of N-Doped Carbon as a Multifunctional Electrocatalyst for ORR, OER, and HER, Adv. Funct. Mater. 1901949 (2019).
[46] Z. Yang, C. Zhao, Y. Qu, H. Zhou, F. Zhou, J. Wang, Y. Wu, Y. Li, Trifunctional Self-Supporting Cobalt-Embedded Carbon Nanotube Films for ORR, OER, and HER Triggered by Solid Diffusion from Bulk Metal, Adv. Mater. 31 (12) (2019) e1808043.
[47] E. Zhang, Y. Xie, S. Ci, J. Jia, P. Cai, L. Yi, Z. Wen, Multifunctional high-activity and robust electrocatalyst derived from metal–organic frameworks, J. Mater. Chem. A 4 (44) (2016) 17288–17298.
[48] Jingshan Luo, Jeong-Hyeok Im, Matthew T. Mayer, Marcel Schreier, Mohammad Khaja Nazeeruddin, Nam-Gyu Park, S. David Tilley, M.G. Hong Jin Fan, Water photolysis at 12.3% efficiencyvia perovskite photovoltaics andEarth-abundant catalysts, science 345(1953) (2014).
[49] Z. Chen, Y. Song, J. Cai, X. Zheng, D. Han, Y. Wu, Y. Zang, S. Niu, Y. Liu, J. Zhu, X. Liu, G. Wang, Tailoring the d-Band Centers Enables Co_4 N Nanosheets To Be Highly Active for Hydrogen Evolution Catalysis, Angew. Chem. Int. Ed. Engl. 57 (18) (2018) 5076–5080.
[50] S. Wan, J. Qi, W. Zhang, W. Wang, S. Zhang, K. Liu, H. Zheng, J. Sun, S. Wang, R. Cao, Hierarchical Co(OH)F Superstructure Built by Low-Dimensional Substructures for Electrocatalytic Water Oxidation, Adv. Mater. 29 (28) (2017).
[51] Z. Kou, Y. Yu, X. Liu, X. Gao, L. Zheng, H. Zou, Y. Pang, Z. Wang, Z. Pan, J. He, S.J. Pennycook, J. Wang, Potential-Dependent Phase Transition and Mo-Enriched Surface Reconstruction of γ-CoOOH in a Heterostructured Co-Mo_2C Precatalyst Enable Water Oxidation, ACS Catal. 10 (7) (2020) 4411–4419.